

Effective Dye Adsorption with Cross-linked Hexagonal Boron Nitride Spheres

Sahra Dandil^{1*}, Abdullah Düzgün¹

Abstract: In this study, cross-linked spheres (CS) were synthesized with chitosan and hexagonal boron nitride (h-BN) to investigate the efficiency of h-BN as an adsorbent and reveal an alternative adsorbent for adsorption processes. CS were used in Reactive Blue 3R (RB3R) and Red P4BN (RP4BN) dye adsorption from wastewater. Surface characteristics of the CS were investigated by Scanning Electron Microscopy (SEM) with Energy Dispersive X-ray (EDX) analysis. The behavior of the adsorption processes with varying effective parameters was investigated. The highest removals were obtained at pH 3 for the RB3R and RP4BN removal processes as 62.8 and 74.2%, respectively. The equilibrium time of the processes was determined as 150 min. The pseudo-first-order kinetic model best explained the adsorption rates of the processes. The Freundlich isotherm model was fitted to define the adsorption mechanisms for both dyes. The positive ΔH values obtained as 24.27 and 16.59 kJ mol⁻¹ for the RB3R and RP4BN adsorption processes, respectively, showed that the processes were endothermic. For the RB3R and RP4BN dye removal processes, ΔS values were calculated as 93.38 and 72.23 J mol⁻¹K⁻¹, respectively. Positive ΔS value indicates the processes that occur with an increase in disorder at the interface. The results described that the CS can be used in the adsorption of RB3R and RP4BN dyes from wastewater.

Keywords: Chitosan, Cross-linked Spheres, Dye Adsorption, Hexagonal Boron Nitride.

¹**Address:** Bilecik Şeyh Edebali University, Faculty of Engineering, Department of Chemical Engineering, 11100, Bilecik, Türkiye.

***Corresponding author:** sahra.ugur@bilecik.edu.tr

Citation: Dandil, S., Düzgün, A. (2023). Effective Dye Adsorption with Cross-linked Hexagonal Boron Nitride Spheres. Bilge International Journal of Science and Technology Research, 7(2): 95-104.

1. INTRODUCTION

Decreased water resources around the world have made the issues of more conscious use of existing resources and reuse of wastewater important. Pollutants that cause a danger to the environment and living things by mixing with wastewater can be exemplified as pesticides, herbicides, pharmaceuticals, heavy metals, industrial dyes and detergents (Peng et al., 2022; Ewis et al., 2022). Among these, dyes cause environmental problems even at very low concentrations. They are preferred for coloring in the textile, leather and paper industries (Duan et al., 2022). Synthetic dyes, which can be ionic (cationic and anionic) and non-ionic, cause serious problems by mixing with water during or after production (Tara et al., 2021; Chouaybi et al., 2022). In addition, their complex molecular structure gives them durability and resistance (Qasem et al., 2022).

Adsorption is one of the preferred effective methods in wastewater treatment. To remove pollutants from wastewater, adsorption describes a mass transfer that occurs

in the form of physical or chemical bonding of dissolved pollutants in the liquid phase (adsorbate) onto a solid phase (adsorbent) (Artioli, 2008; Liyanag and Walpita, 2020; Hu and Xu, 2020). The method is frequently preferred for industrial dye removal due to its low cost, controllability and high performance.

One of the most researched aspects of the adsorption method is the synthesis of new adsorbents. The adsorbents to be used in adsorption processes are expected to be high-capacity, porous, cheap and stable, and provide high efficiency. One of the materials frequently used in adsorbent synthesis is chitosan. Chitosan is a natural polysaccharide synthesized by the N-deacetylation of chitin (Chen et al., 2022). Chitosan has applications in adsorption because it can interact with pollutants with amino (-NH₂) and hydroxyl (-OH) groups in its molecules (Verma and Dutta, 2020). Synthesis of various adsorbents using chitosan and their use in different adsorption processes are included in the literature. Among the studies in recent years, Chen et al. synthesized chitosan-based aerogel and used it in thorium adsorption (Chen et al.,

2022). Yeo et al. synthesized bentonite-chitosan composites for use in the removal of antibiotics (Yeo et al., 2023). Wang et al. prepared magnetic chitosan using chitosan and iron oxide (Fe_3O_4) as an adsorbent and used it in dye adsorption (Wang et al., 2022). Xu et al. studied the adsorption of heavy metals with composite beads synthesized with paper waste and chitosan (Xu et al., 2022).

It is known that two-dimensional materials have excellent electrical, mechanical and thermal properties compared to their bulk forms (An et al., 2022). Hexagonal boron nitride (h-BN) is a two-dimensional material with a structure similar to graphene (Yun et al., 2022). h-BN has many uses with its excellent mechanical, electrical, thermal and chemical properties (Chen et al., 2022). In this study; in order to investigate the efficiency of h-BN in wastewater treatment and to reveal an alternative adsorbent that can be used in adsorption processes, cross-linked spheres (CS) containing h-BN and chitosan were synthesized and used in dye adsorption processes. This study is important in terms of examining the usability of h-BN, which draws attention to its superior properties, as an adsorbent in adsorption processes, in addition to its usage areas. Reactive Blue 3R (RB3R) and Red P4BN (RP4BN) dyes were chosen as dyes. RB3R (C.I. Reactive Blue 28) belongs to the vinyl sulfone dye group (Emco, 2023). RP4BN (C.I. Reactive Red 3.1) is also in a reactive dye group (Aditya, 2023). The effective parameters (pH, time, dye concentration, adsorbent dosage and temperature) of both dye removal processes were examined. Kinetic, equilibrium and thermodynamic data of the processes were performed to describe the RB3R and RP4BN dye adsorption by the spheres.

2. MATERIAL AND METHOD

2.1. Materials

Chitosan and hexagonal boron nitride (h-BN) were used to synthesize cross-linked spheres (CS) to use as an adsorbent. h-BN (micron size) was supplied from BORTEK. The acetic acid solution was purchased from Merck. Glutaraldehyde solution (50%) was used as a cross-linker and supplied from Fluka. RB3R and RP4BN dyes used as adsorbates were obtained from a textile dye production factory in Turkey. Various concentrations of hydrochloric acid (HCl) and sodium hydroxide (NaOH) solutions were used to adjust the pH of the dye solutions.

2.2. Synthesis and characterization of adsorbent

Synthesis of the adsorbent was carried out similarly to the study previously presented by Dandil et al (Dandil et al., 2019). 1.5 g chitosan was added to 75 mL of 5% by volume acetic acid solution and left to stir overnight. After mixing was complete, 0.5 g of h-BN was added to the mixture and stirred overnight. The mixture was added to a 1M NaOH solution with a syringe. It was observed that each drop of the mixture became spherical particles. The spheres were left to mix overnight. Then, the spheres were washed with distilled water. Several washes were continued until pH 7. The spheres were added to a 2.5% glutaraldehyde - ethyl alcohol solution by mass and kept in a shaker at 60 °C for 15 hours. The spheres washed with distilled water were held at -80 °C

for a night. Then the spheres were kept in a freeze-dryer for 24 hours.

The surface characteristics of the CS were determined with Scanning Electron Microscopy (SEM) analysis. Zeiss Supra 40VP was used to investigate the surface porosity and pore distribution of the sample. Also, Energy Dispersive X-ray (EDX) technique was performed for the chemical characterization of the CS.

2.3. Adsorption

The synthesized spheres were used for the adsorption of RB3R and RP4BN dyes from aqueous solutions. The effective parameters such as pH (3-9), time (0-150 min), dye concentration (25-150 ppm), adsorbent dosage (0.2-0.8 g/L) and temperature (25-45 °C) on the removal processes were investigated. The same parameter values were studied for both dyes.

Adsorption studies were carried out with 50 mL dye solutions. The aqueous dye solutions were prepared with deionized water. The experiments were performed in a shaker (Thermal H11960) at 200 rpm. Absorbance values of the samples taken at certain time intervals to determine the dye concentrations in aqueous solutions were obtained with the Ultraviolet-Visible region (UV-GB) spectrophotometer (Perkin Elmer, Elmer Analyst 800) at a wavelength of 585 and 535 nm, where the maximum absorbance values for RB3R and RP4BN dyes was observed, respectively.

The adsorption data of the processes were studied with the adsorption capacity and removal percentage equations given below (Long et al., 2022):

$$q_e = \frac{(C_0 - C_e) \times V}{m} \quad (1)$$

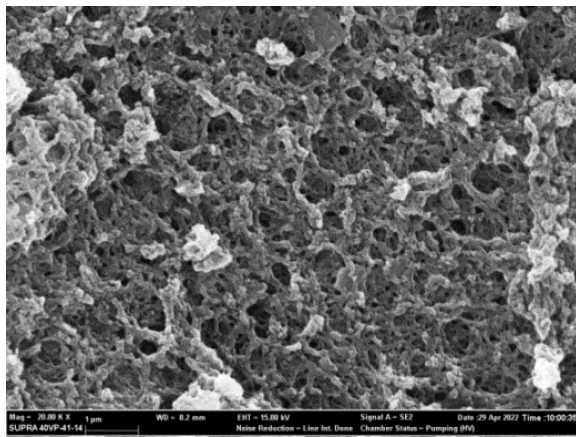
$$\% \text{Removal} = \frac{(C_0 - C_e) \times 100}{C_0} \quad (2)$$

where q_e ; the amount of dye adsorbed at equilibrium (mg g^{-1}), C_0 and C_e ; initial and equilibrium dye concentrations of dye solution (mg L^{-1}), respectively, V ; volume (L), m ; adsorbent mass (g) (Long et al., 2022).

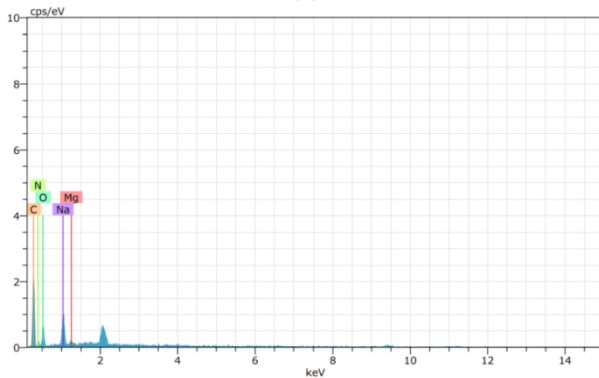
3. RESULTS AND DISCUSSION

3.1. Characterization of the spheres

The surface characteristics of the CS were observed by SEM images. SEM micrograph of the CS at 20000 magnifications is presented in Figure 1 (a). The porous and uniform texture of the spheres is shown in microscopic observation. The elemental composition of the adsorbent was examined by EDX analysis. As given in Figure 1 (b), carbon (C) and oxygen (O) elements were observed in the EDX image of the CS. According to the quantitative analysis of the CS given in Table 1, the mass fraction of C and O are determined as 51.21 and 25.78%, respectively.



(a)



(b)

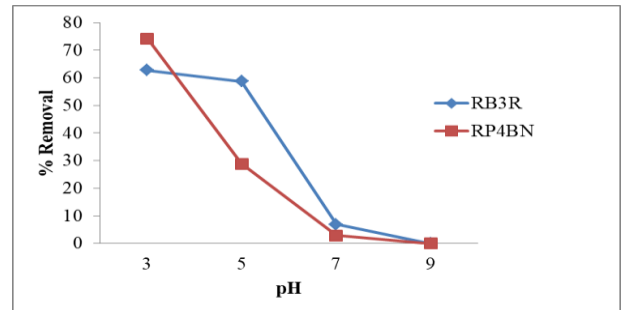
Figure 1. (a) SEM and (b) EDX images of the CS**Table 1.** Quantitative results of EDX analysis for the CS

Elements	Mass%	Atomic%
Carbon	51.21	59.30
Oxygen	25.78	22.41
Sodium	11.05	6.68
Nitrogen	11.31	11.23
Magnesium	0.66	0.38

3.2. Effect of pH of the dye solutions and contact time

The pH of the RB3R and RP4BN dye solutions has a great effect on the adsorption processes due to changing the surface charge of the CS. The surface charge of an adsorbent is significant since it affects the adherence of the ionized RB3R and RP4BN dye molecules on the CS surface. To investigate the effect of various pH values on the RB3R and RP4BN dye adsorption on the CS, experiments were done for pH values in the range of 3-9 of dye solutions. The concentration of the dye solutions was 50 ppm, the adsorbent dosage was 0.4 g/L and the temperature was 25 °C in the experiments. The processes were followed for 150 minutes. pH effect on the removal percentages of RB3R and RP4BN dyes by the CS is given in Figure 2. According to Figure 2, it was observed that RB3R and RP4BN removal percentages decreased with the increase of pH values from 3 to 7, and no removal occurred for both dyes at pH 9. The percentages of RB3R dye removal by the CS were determined as 62.8, 58.7 and 6.9% at pH of 3, 5 and 7, respectively. And also for the RP4BN dye adsorption process from aqueous solution 74.2, 28.8 and 2.8% removal efficiencies were observed at pH of

3, 5 and 7, respectively. Thus, the effect of pH on adsorption was confirmed. The highest removals were obtained at pH 3 for both processes. Due to the positive charge density in the aqueous solution medium at pH 3, the adsorption of anionic RB3R and RP4BN dyes on the CS was effective. As the pH increased, the adsorption efficiencies of the dyes decreased with the decrease of the positively charged sites (Mahmoodi and Mokhtari-Shourijeh, 2015).

**Figure 2.** Effect of pH on the removal percentages of RB3R and RP4BN dyes by the CS (Initial dye concentrations: 50 mg/L, adsorbent dosage: 0.4 g/L, temperature: 25 °C, time: 150 min)

The RB3R and RP4BN adsorption processes on the CS were followed with time in the range of pH 3-9 of the dye solutions and results were given in Figure 3. According to the graphs given in Figure 3 (a) and (b) for RB3R and RP4BN dye removal processes, respectively, regular increases were observed in the removal percentages for both dyes over time at all pH values. After 90 minutes for both processes, the increase in removal percentages started to decrease and the processes reached equilibrium in 150 minutes at pH 3, where the highest removal was determined. Also, a higher removal of RP4BN dye (74.2%) than RB3R dye (62.8%) was obtained at pH 3 in 150 minutes. In the early times of adsorption, the unoccupied sites of the CS allowed more efficient and rapid adsorption of the RB3R and RP4BN molecules. However, due to the active sites that start to occupy the dye molecules with time, the removal percentages decrease and reach an equilibrium where there is no dye removal (Wong et al., 2020).

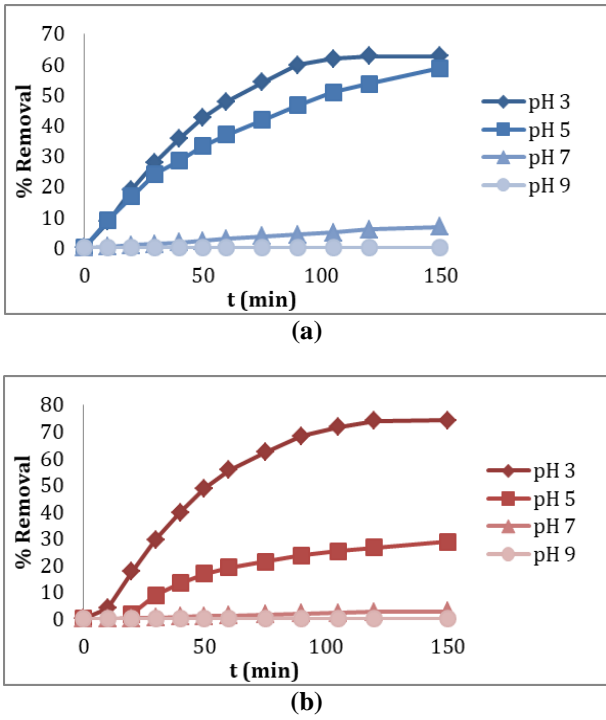


Figure 3. Effect of contact time on the removal percentages of (a) RB3R and (b) RP4BN dyes by the CS (Initial dye concentrations: 50 mg/L, adsorbent dosage: 0.4 g/L, temperature: 25 °C)

3.3. Adsorption kinetics

The experimental data obtained for the RB3R and RP4BN dye adsorption with the synthesized spheres were evaluated with the two most used kinetic models. The adsorption kinetics of the dye adsorption processes were studied with the pseudo-first-order and pseudo-second-order models.

The pseudo-first-order and pseudo-second-order kinetic model equations were presented in Equations (3) and (4), respectively (Loganathan et al., 2022):

$$\log(q_e - qt) = \log q_e - \frac{k_1}{2.303}t \tag{3}$$

$$\frac{t}{qt} = \frac{1}{k_2 q_e^2} + \frac{t}{q_e} \tag{4}$$

where t; time (min), qt; adsorbed dye at time t (mg g⁻¹), k₁ and k₂; first-order kinetic model rate constant (min⁻¹) and second-order kinetic model rate constant (g mg⁻¹ min⁻¹), respectively and C; constant (Loganathan et al., 2022).

The pseudo-first-order and pseudo-second-order kinetic model plots of the RB3R and RP4BN dye removal processes by the CS are seen in Figure 4 (a) and (b), respectively. The parameters of the kinetic models were also presented in Table 2. The correlation coefficients (R²) of the RB3R and RP4BN adsorption processes seen in Table 2 were interpreted to decide on the kinetic model that best describes the processes. The R² values of the pseudo-first-order kinetic model were higher than the R² values of the second-order kinetic model for both dyes. Thus, the pseudo-first-order

kinetic model was found as compatible with the removal of RB3R and RP4BN dyes by the CS. The highest R² values of the pseudo-first-order model indicate the RB3R and RP4BN dye removal processes by the CS occur physically (Zaini et al., 2022). In addition, the calculated q_e value for the RP4BN dye was found to be higher than that of the RB3R dye.

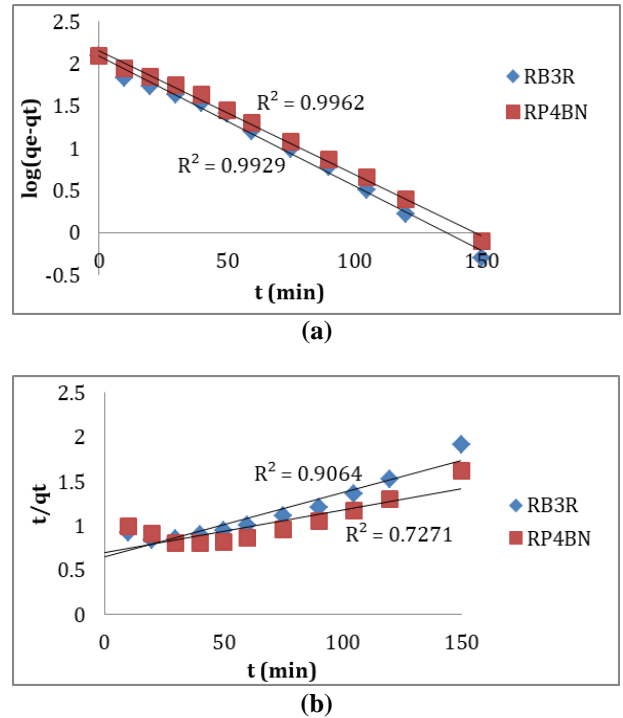


Figure 4. (a) Pseudo-first-order, and (b) pseudo-second-order kinetic model plots for the RB3R and RP4BN dye adsorption processes

Table 2. Kinetic parameters of the RB3R and RP4BN dye adsorption processes

	Pseudo-First-Order Kinetic Model			Pseudo-Second-Order Kinetic Model		
	k ₁ (x10 ²) (min ⁻¹)	q _{e,cal} (mg g ⁻¹)	R ²	k ₂ (x10 ⁵) (g mg ⁻¹ min ⁻¹)	q _{e,cal} (mg g ⁻¹)	R ²
RB3R	3.55	125.6	0.992	7.98	138.8	0.906
RP4B	3.36	142.3	0.996	3.30	208.3	0.727
N		3	2		3	1

3.4. Effect of initial concentration of the dye solutions and isotherm studies

To examine the dye concentration effect on removal efficiency, the adsorption processes of RB3R and RP4BN dyes on the CS were studied in the range of 25-150 ppm dye solution concentrations. The processes were followed at 0.4 g/L adsorbent dosage and 25 °C for 150 minutes. The effect of initial dye concentration on the removal percentages of the processes is given in Figure 5. In Figure 5 (a) and (b), it is observed that the removal efficiencies increase over time for each concentration according to the graphs showing the change in the percentage of removal of RB3R and RP4BN dyes, respectively. At the end of 150 minutes, 48.0, 62.8,

67.6 and 42.1% removals were obtained for RB3R dye at 25, 50, 100 and 150 ppm, respectively. Removal percentages of 63.3, 74.2, 71.2 and 63.0% were obtained for RP4BN at 25, 50, 100 and 150 ppm, respectively. It is seen that higher removals were obtained for RP4BN than RB3R at all concentration values. For both dyes, the removal percentages increased with increasing dye concentration but decreased after a high concentration. Up to a certain concentration, the number of unoccupied sites for adsorption is high, and the driving force for mass transfer also increases. After a high concentration, the removal efficiency decreases as the number of sites required to increase the concentration will be limited. The results agree with other adsorption studies presented previously (Pathania et al., 2017; Salimi et al., 2017; Farouq, 2022;).

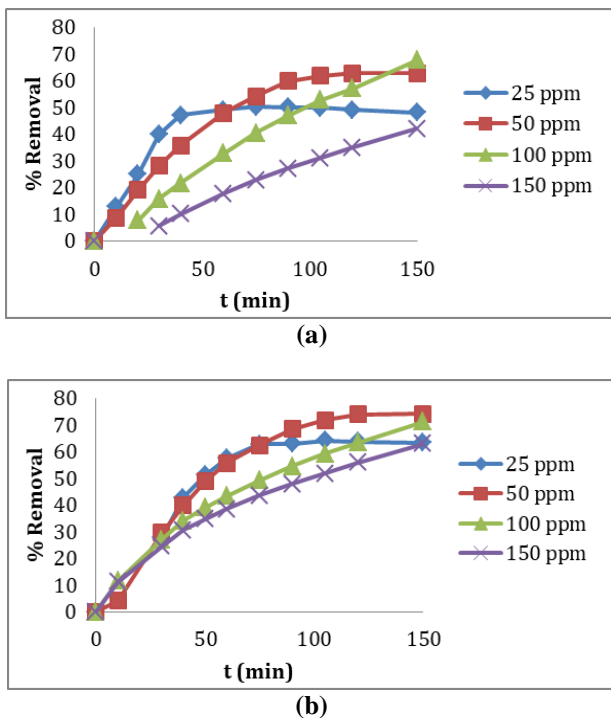


Figure 5. Effect of initial concentrations of (a) RB3R and (b) RP4BN dye solutions on the removal efficiencies of the RB3R and RP4BN dye adsorption processes (Adsorbent dosage: 0.4 g/L, time: 150 min, temperature: 25 °C)

Langmuir and Freundlich models were studied to explain the mechanisms of the RB3R and RP4BN dye adsorption processes on the spheres. Langmuir and Freundlich equations are given below respectively (Dandil et al., 2019):

$$\frac{C_e}{q_e} = \frac{C_e}{q_m} + \frac{1}{(q_m K_L)} \quad (5)$$

$$\ln q_e = \ln K_F + \frac{1}{n} \ln C_e \quad (6)$$

where K_L ; Langmuir isotherm constant ($L g^{-1}$), q_m ; maximum adsorption capacity ($mg L^{-1}$), K_F ; Freundlich isotherm constant, and n ; linearity constant for Freundlich isotherm (Dandil et al., 2019).

The plots of Langmuir and Freundlich isotherm are seen in Figure 6. In addition, the isotherm parameters of both

processes were calculated and presented in Table 3. As given in Table 3, the R^2 values of the isotherm models exhibit that the Freundlich isotherm model clarifies better isotherm studies of both processes than the Langmuir model. The Freundlich isotherm model for the RB3R and RP4BN dye removal processes describes that the RB3R and RP4BN dye is adsorbed on the surface of the CS with multilayer sorption (Salim et al., 2021). The n value indicates the heterogeneity of the CS surface and being below unity explains cooperative adsorption (Ojediran et al., 2021; Salim et al., 2021).

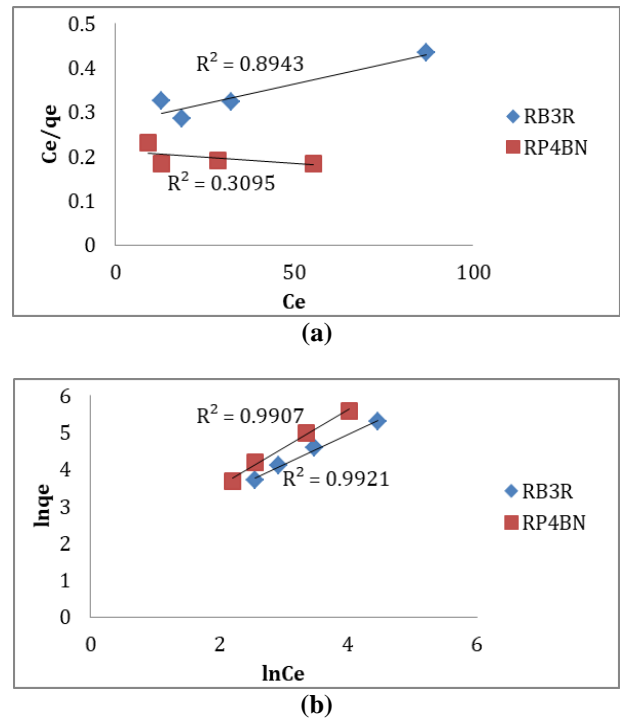


Figure 6. (a) Langmuir and (b) Freundlich isotherms for the RB3R and RP4BN dye adsorption processes

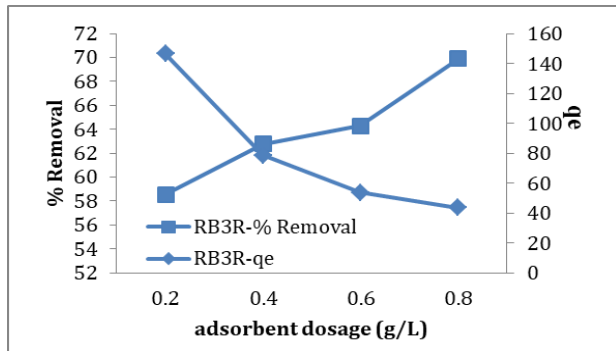
Table 3. Freundlich and Langmuir isotherm model parameters for the RB3R and RP4BN dye adsorption processes

	Langmuir Isotherm			Freundlich Isotherm		
	$K_L(x10^3)$ (L/mg)	$q_m(x10^3)$ (mg g ⁻¹)	R^2	K_F (mg g ⁻¹ (L/g) ^{1/n})	n	R^2
RB3R	6.55	0.55	0.8943	5.16	1.206	0.9921
RP4BN	-2.8	-1.67	0.3095	4.23	0.956	0.9907

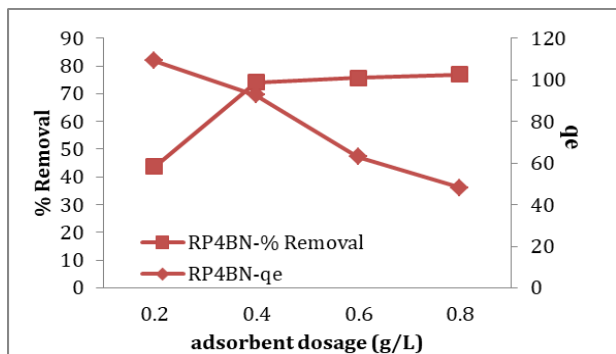
3.5. Effect of adsorbent dosage

To investigate the CS amount effect on the RB3R and RP4BN dye removal processes, studies were performed at various adsorbent dosages (0.2-0.8 g/L). Data were obtained for 150 minutes at 25 °C at a concentration of 50 ppm dye solutions. The behavior of RB3R and RP4BN dye removal processes at different adsorbent dosages are given in Figure 7 (a) and (b), respectively. For both processes, the removal percentages increased with the increasing adsorbent dosage, while the adsorption capacities decreased. For the RB3R dye adsorption process, increasing CS dosage from 0.2 to 0.8 g/L increased the RB3R dye removal percentage from 58.6 to 69.9%, but decreased the adsorption capacity from 146.4 to

43.7 mg/g. Similarly, the RP4BN dye removal increased with the CS dosage from 43.6 to 76.9%, while the adsorption capacity decreased from 109.1 to 48.1 mg/g. Increasing the adsorbent dosage above 0.4 g/L slightly increased the removal percentages of RP4BN (Figure 7 (b)), but effectively increased it for RB3R removal (Figure 7 (a)). In addition, the adsorbent dosage showed a strong effect on the adsorption capacity of both dyes.



(a)



(b)

Figure 7. Effect of adsorbent dosage on the removal efficiencies and adsorption capacities in (a) RB3R and (b) RP4BN dye adsorption processes (Initial dye concentrations: 50 mg/L, time: 150 min, temperature: 25 °C)

Table 4 presents the adsorption capacities of some adsorbents prepared using chitosan in previous studies with the CS in dye removal processes. According to Table 4, CS has a moderate adsorption capacity compared to other studies in the literature.

Table 4. Adsorption capacities of adsorbents synthesized with chitosan in dye removal

Adsorbent	Dye	Adsorption capacity (mg g ⁻¹)	Reference
salicylaldehyde functionalized chitosan	Crystal violet	6.85	Parshi et al., 2019
	Rose Benga	15.26	
chitosan-Gelatin / zirconium (IV) selenophosphate nanocomposite	Methylene blue	10.46	Kaur and Jindal, 2019
CS	RB3R	146.4	Present study
	RP4BN	109.1	
photocatalytic flyash/TiO ₂ modified chitosan biopolymer composite	Congo red	163.51	Gajera et al., 2022
	Methylene blue	55.75	
chitosan-montmorillonite hydrogel beads	methyl green	303.21	Kurczewska, 2022
magnetic Fe ₃ O ₄ embedded chitosan-crosslinked-polyacrylamide composites	Sunset yellow	359.71	Jiang et al., 2022
MIL-53(Fe)/chitosan composite hydrogel spheres	Congo red	590.8	Jin et al., 2022
chitosan-based dual network composite hydrogel	Methylene blue	596.14	Wan et al., 2022

3.6. Effect of temperature and thermodynamics

The temperature effect on the RB3R and RP4BN dye removal processes was investigated at 25, 35, and 45 °C with 0.4 g/L adsorbent dosage at 50 ppm initial dye concentrations for 150 min. The equations given below are used to calculate thermodynamic parameters (Raghav and Kumar, 2018):

$$\ln K_d = \frac{\Delta S}{R} - \frac{\Delta H}{RT} \quad (7)$$

$$K_d = \frac{q_e}{C_e} \quad (8)$$

$$\Delta G = \Delta H - T\Delta S \quad (9)$$

where K_d ; adsorption equilibrium constant, ΔS ; entropy (J mol⁻¹K⁻¹), ΔH ; enthalpy (kJ mol⁻¹), ΔG ; Gibb's free energy (kJ mol⁻¹), R ; gas constant (8.314 J mol⁻¹ K⁻¹), T ; temperature (K) (Raghav and Kumar, 2018).

The Van't Hoff plot showing the relationship between temperature and equilibrium constant is shown in Figure 8. In addition, the thermodynamic parameters of both processes are given in Table 5 with the parameters of similar processes. According to Table 5, the positive enthalpy change values indicate the RB3R and RP4BN dye removal processes by the CS are endothermic (Rios-Donato et al., 2017). It is known that weak van der Waals forces are effective in bonding when the ΔH is below 25 kJ mol⁻¹ and strong chemical bonds are effective when it is in the range of 40-200 kJ mol⁻¹ (de Oliveira et al., 2023). $\Delta S > 0$ shows the processes that occur with an increase in disorder at the interface (Doke and Khan, 2013). According to the ΔS values in Table 5, a more disordered state at the interface can be mentioned for the RB3R adsorption process (93.38 J mol⁻¹K⁻¹) compared to the RP4BN process (72.23 J mol⁻¹K⁻¹). For both processes, negative ΔG values were found at the temperatures studied. The decrease in these values with increasing temperature

explains more effective dye removal at high temperatures (Batool et al., 2018).

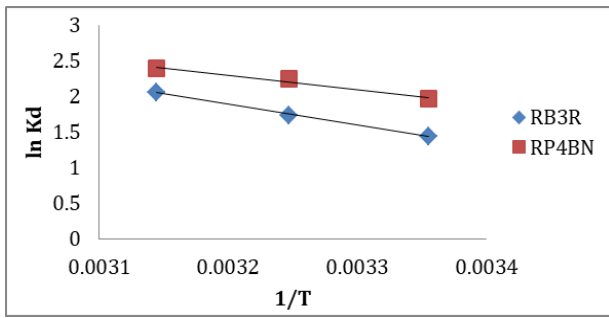


Figure 8. Van't Hoff plots of the RB3R and RP4BN dye adsorption processes

Table 5. Thermodynamic parameters of the RB3R and RP4BN dye adsorption processes and similar studies

Adsorbent	Dye	T (K)	ΔG^0 (kJ mol ⁻¹)	ΔH^0 (kJ mol ⁻¹)	ΔS^0 (J mol ⁻¹ K ⁻¹)	Ref.
chitosan composite of metal-organic framework	Methylene blue	298	9.203	-9.628	-63	Saeed et al., 2022
		308	9.834			
		318	10.466			
	Methyl orange	298	9.400	-19.588	-97	
		308	10.373			
		318	11.346			
polyethyleneimine-modified chitosan/Ce-UIO-66 composite	Methyl orange	303	-3.805	-15.954	-40.097	Chen et al., 2023
		313	-3.404			
		323	-3.003			
		333	-2.602			
		343	-2.201			
MIL-53(Fe)/chitosan composite hydrogel spheres	Congo red	298	-37.63	-5.60	-107.5	Jin et al., 2023
		308	-38.75			
		318	-39.79			
micro/nano MIL-88A (Fe, Al, Fe-Al)/chitosan composite sponge	MIL-88A (Fe-Al)/CS	298	-31.68	83.65	385.4	Zhao et al., 2023
		308	-34.06			
		318	-39.45			
	MIL-88A (Fe)/CS	298	-32.58	75.10	359.6	
		308	-34.51			
		318	-39.84			
	MIL-88A (Al)/CS	298	-32.93	79.34	374.9	
		308	-34.98			
		318	-40.50			
fibrous chitosan/sodium alginate composite foams	CSA1-1	298	-22.03	1.53	79.06	Zhao et al., 2021
		308	-22.82			
		318	-23.61			
	CSA1-5	298	-16.60	5.07	72.73	
		308	-17.33			
		318	-18.06			
citric acid-crosslinked Zn-MOF/chitosan composite	Methyl orange	298	-5.698	-33.448	-55.967	Niu et al., 2021
		308	-5.301			
		318	-4.653			
CS	RB3R	298	-3.55	24.27	93.38	Present study
		308	-4.48			
		318	-5.42			
	RP4BN	298	-4.93	16.59	72.23	
		308	-5.65			
		318	-6.37			

4. CONCLUSIONS

In the study, the usability of the spheres obtained by cross-linking chitosan and h-BN (CS) as an adsorbent was investigated. Also, the efficiency of h-BN as an adsorbent in adsorption processes is presented. The synthesized spheres were used to remove RB3R and RP4BN dyes from wastewater. According to pH effect studies, it was determined that the highest removals were obtained at pH 3 for the RB3R and RP4BN dye removal processes, as 62.8 and 74.2%, respectively. The equilibrium time of the processes was determined as 150 minutes. The pseudo-first-order kinetic model best explained the adsorption rates of the processes. The Freundlich isotherm model is best fitted to define the adsorption mechanisms for both dyes. ΔH values for RB3R and RP4BN dye adsorption processes were calculated as 24.27 and 16.59 kJ mol⁻¹, respectively and clarified that the processes were endothermic. For the RB3R and RP4BN dye removal processes, ΔS values were determined as 93.38 and 72.23 J mol⁻¹K⁻¹, respectively. Positive ΔS values indicate the processes that occur with an increase in disorder at the interface. Negative ΔG values show spontaneous adsorption for both dyes. As a result, the CS showed effectiveness as an adsorbent in RB3R and RP4BN dye adsorption processes.

Author Contributions

Conceptualization: S.D.; Investigation: S.D.; Material and Methodology: S.D., A.D.; Supervision: S.D.; Visualization: S.D.; Writing-Original Draft: S.D.; Writing-review & Editing: S.D., A.D.; Other: All authors have read and agreed to the published version of manuscript.

Conflict of Interest

The authors have no conflicts of interest to declare.

Funding

Bilecik Seyh Edebali University Scientific Research Projects Coordinator ship supported the study with the project code 2021-02.BŞEÜ.03-03.

REFERENCES

- Aditya Color Chem, <https://www.adityacolorchem.com/products/reactive-dyes.html>, (Accessed April 16, 2023)
- An, L., Gu, R., Zhong, B., Yu, Y., Zhang, J. (2022). Water-icing-triggered scalable and controllable exfoliation of hexagonal boron nitride nanosheets. *Cell Reports Physical Science*, 3(7), 100941. <https://doi.org/10.1016/j.xcrp.2022.100941>
- Artioli, Y. (2008). Adsorption, in: Jørgensen, S. E. and Fath, B. D. (Eds.), *Encyclopedia of Ecology*. Elsevier, Amsterdam, Netherlands, pp. 60-65. <https://doi.org/10.1016/B978-008045405-4.00252-4>
- Batool, F., Akbar, J., Iqbal, S., Noreen, S., Bukhari, S. N. A. (2018). Study of isothermal, kinetic, and thermodynamic parameters for adsorption of cadmium: an overview of linear and nonlinear approach and error analysis. *Bioinorganic chemistry and applications*, 2018. <https://doi.org/10.1155/2018/3463724>.
- Chen, B., Ding, L., Wang, Y., Zhang, Y. (2022). High efficient adsorption for thorium in aqueous solution using a novel tentacle-type chitosan-based aerogel: Adsorption behavior and mechanism. *International Journal of Biological Macromolecules*, 222, 1747-1757. <https://doi.org/10.1016/j.ijbiomac.2022.09.256>
- Chen, C., Wang, G., Beshiwork, B. A., Xu B., Lin B. (2022). Strain-tunable pure H⁻ conduction in one-atom-thick hexagonal boron nitride for high-energy-density fuel cells. *Chemical Engineering Journal*, 450, 138223. <https://doi.org/10.1016/j.cej.2022.138223>
- Chen, S., Tian, H., Mao, J., Ma, F., Zhang, M., Chen, F., Yang, P. (2022). Preparation and application of chitosan-based medical electrospun nanofibers. *International Journal of Biological Macromolecules*, 226, 410-422, 2022. <https://doi.org/10.1016/j.ijbiomac.2022.12.056>
- Chen, Z., Zhang, Z. B., Zeng, J., Zhang, Z. J., Ma, S., Tang, C. M., Xu, J. Q. (2023). Preparation of polyethyleneimine-modified chitosan/Ce-UIO-66 composite hydrogel for the adsorption of methyl orange. *Carbohydrate Polymers*, 299, 120079. <https://doi.org/10.1016/j.carbpol.2022.120079>
- Chouaybi, I., Ouassif, H., Bettach, M., Moujahid, E. M. (2022). Fast and high removal of acid red 97 dye from aqueous solution by adsorption onto a synthetic hydrocalumite: Structural characterization and retention mechanisms. *Inorganic Chemistry Communications*, 146, 110169. <https://doi.org/10.1016/j.inoche.2022.110169>
- Dandil, S., Sahbaz, D. A., Acikgoz, C. (2019). Adsorption of Cu (II) ions onto crosslinked chitosan/Waste Active Sludge Char (WASC) beads: Kinetic, equilibrium, and thermodynamic study. *International journal of biological macromolecules*, 136, 668-675. <https://doi.org/10.1016/j.ijbiomac.2019.06.063>
- de Oliveira, T. F., de Souza, C. P., Lopes-Moriyama, A. L., da Silva, M. L. P. (2023). In situ modification of MCM-41 using niobium and tantalum mixed oxide from columbite processing for methylene blue adsorption: Characterization, kinetic, isotherm, thermodynamic and mechanism study. *Materials Chemistry and Physics*, 294, 127011. <https://doi.org/10.1016/j.matchemphys.2022.127011>
- Doke, K. M., Khan, E. M. (2013). Adsorption thermodynamics to clean up wastewater; critical review. *Reviews in Environmental Science and Bio/Technology*, 12(1), 25-44. DOI 10.1007/s11157-012-9273-z
- Duan, Y. T., Yao, Y., Ameta, R. K. (2022). Removal and recovering of anionic and cationic dyes using Neem Leaf ash prepared at 250, 500 and 750° C: Analyzed by adsorption isotherm and physicochemical parameters. *Journal of Molecular Liquids*, 370, 121012. <https://doi.org/10.1016/j.molliq.2022.121012>

- Emco Dyestuff Pvt. Ltd., <https://www.emcochemicals.com/Dyes/Reactive-Dyes/Reactive-Dyes-VINYL-SULPHONE/Blue-3R> (Accessed April 16, 2023)
- Ewis, D., Ba-Abbad, M. M., Benamor, A., El-Naas, M. H. (2022). Adsorption of organic water pollutants by clays and clay minerals composites: A comprehensive review. *Applied Clay Science*, 229, 106686. <https://doi.org/10.1016/j.clay.2022.106686>
- Farouq, R. (2022). Coupling Adsorption-Photocatalytic Degradation of Methylene Blue and Maxilon Red. *Journal of Fluorescence*, 32(4), 1-8. <https://doi.org/10.1007/s10895-022-02934-1>
- Gajera, R., Patel, R. V., Yadav, A., Labhasetwar, P. K. (2022). Adsorption of cationic and anionic dyes on photocatalytic flyash/TiO₂ modified chitosan biopolymer composite. *Journal of Water Process Engineering*, 49, 102993. <https://doi.org/10.1016/j.jwpe.2022.102993>
- Hu, H., Xu, K. (2020). Physicochemical technologies for HRPs and risk control, in: Ren, H. and Zhang, X. (Eds.), *High-risk pollutants in wastewater*. Elsevier, Amsterdam, Netherlands, pp. 169-207. <https://doi.org/10.1016/B978-0-12-816448-8.00008-3>
- Jiang, R., Shen, T. T., Zhu, H. Y., Fu, Y. Q., Jiang, S. T., Li, J. B., Wang, J. L. (2022). Magnetic Fe₃O₄ embedded chitosan-crosslinked-polyacrylamide composites with enhanced removal of food dye: Characterization, adsorption and mechanism. *International Journal of Biological Macromolecules*, 227, 1234-1244. <https://doi.org/10.1016/j.ijbiomac.2022.11.310>
- Jin, Y., Li, Y., Du, Q., Chen, B., Chen, K., Zhang, Y., Wang, M., Sun, Y., Zhao, S., Jing, Z., Wang, Y. (2022). Efficient adsorption of Congo red by MIL-53 (Fe)/chitosan composite hydrogel spheres. *Microporous and Mesoporous Materials*, 348, 112404. <https://doi.org/10.1016/j.micromeso.2022.112404>
- Jin, Y., Li, Y., Du, Q., Chen, B., Chen, K., Zhang, Y., Wang, M., Sun, Y., Zhao, S., Jing, Z., Wang, J. (2023). Efficient adsorption of Congo red by MIL-53 (Fe)/chitosan composite hydrogel spheres. *Microporous and Mesoporous Materials*, 348, 112404. <https://doi.org/10.1016/j.micromeso.2022.112404>
- Kaur, K., Jindal, R. (2019). Comparative study on the behaviour of Chitosan-Gelatin based Hydrogel and nanocomposite ion exchanger synthesized under microwave conditions towards photocatalytic removal of cationic dyes. *Carbohydrate Polymers*, 207, 398-410. <https://doi.org/10.1016/j.carbpol.2018.12.002>
- Kurczewska, J. (2022). Chitosan-montmorillonite hydrogel beads for effective dye adsorption. *Journal of Water Process Engineering*, 48, 102928. <https://doi.org/10.1016/j.jwpe.2022.102928>
- Liyanage, D., Walpita, J. (2020). Organic pollutants from E-waste and their electrokinetic remediation. in: Prasad, M.N.V., Vithanage, M. and Borthakur, A. (Eds.), *Handbook of Electronic Waste Management*. Elsevier, Amsterdam, Netherlands, pp. 171-189.
- Loganathan, M., Raj, A. S., Murugesan, A., Kumar, P. S. (2022). Effective adsorption of crystal violet onto aromatic polyimides: Kinetics and isotherm studies. *Chemosphere*, 304, 135332. <https://doi.org/10.1016/j.chemosphere.2022.135332>
- Long, W., Yang, C., Wang, G., Hu, J. (2022). Effective adsorption of Hg (II) ions by new ethyleneimine polymer/ β -cyclodextrin crosslinked functionalized magnetic composite. *Arabian Journal of Chemistry*, 104439. <https://doi.org/10.1016/j.arabjc.2022.104439>
- Mahmoodi, N. M., Mokhtari-Shourijeh, Z. (2015). Preparation of PVA-chitosan blend nanofiber and its dye removal ability from colored wastewater. *Fibers and Polymers*, 16(9), 1861-1869. DOI 10.1007/s12221-015-5371-1
- Niu, C., Zhang, N., Hu, C., Zhang, C., Zhang, H., Xing, Y. (2021). Preparation of a novel citric acid-crosslinked Zn-MOF/chitosan composite and application in adsorption of chromium (VI) and methyl orange from aqueous solution. *Carbohydrate Polymers*, 258, 117644. <https://doi.org/10.1016/j.carbpol.2021.117644>
- Ojediran, J. O., Dada, A. O., Aniyi, S. O., David, R. O., Adewumi, A. D. (2021). Mechanism and isotherm modeling of effective adsorption of malachite green as endocrine disruptive dye using Acid Functionalized Maize Cob (AFMC). *Scientific reports*, 11(1), 1-15. | <https://doi.org/10.1038/s41598-021-00993-1>
- Parshi, N., Pan, D., Dhavle, V., Jana, B., Maity, S., Ganguly, J. (2019). Fabrication of lightweight and reusable salicylaldehyde functionalized chitosan as adsorbent for dye removal and its mechanism. *International journal of biological macromolecules*, 141, 626-635. <https://doi.org/10.1016/j.ijbiomac.2019.09.025>
- Pathania, D., Sharma, S., Singh, P. (2017). Removal of methylene blue by adsorption onto activated carbon developed from Ficus carica bast. *Arabian journal of chemistry*, 10, S1445-S1451. <https://doi.org/10.1016/j.arabjc.2013.04.021>
- Peng, R., Zhang, S., Yao, Y., Wang, J., Zhu, X., Jiang, R., Zhang, J., Zhang, W., Wang, C. (2022). MOFs meet electrospinning: new opportunities for water treatment. *Chemical Engineering Journal*, 453, 139669. <https://doi.org/10.1016/j.cej.2022.139669>
- Qasem, K. M., Khan, S., Chinnam, S., Saleh, H. A., Mantasha, I., Zeeshan, M., Manea, Y. K., Shahid, M. (2022). Sustainable fabrication of Co-MOF@ CNT nano-composite for efficient adsorption and removal of organic dyes and selective sensing of Cr (VI) in aqueous phase. *Materials Chemistry and Physics*,

- 291, 126748.
<https://doi.org/10.1016/j.matchemphys.2022.126748>
- Raghav, S., Kumar, D. (2018). Adsorption equilibrium, kinetics, and thermodynamic studies of fluoride adsorbed by tetrametallic oxide adsorbent. *Journal of Chemical & Engineering data*, 63(5), 1682-1697. <https://doi.org/10.1021/acs.jced.8b00024>
- Rios-Donato, N., Peña-Flores, A. M., Katime, I., Leyva-Ramos, R., Mendizábal, E. (2017). Kinetics and thermodynamics of adsorption of red dye 40 from acidic aqueous solutions onto a novel chitosan sulfate. *Afinidad*, 74(579), 214-220. <https://raco.cat/index.php/afinidad/article/view/328558/419163>
- Saeed, T., Naeem, A., Din, I. U., Farooq, M., Khan, I. W., Hamayun, M., Malik, T. (2022). Synthesis of chitosan composite of metal-organic framework for the adsorption of dyes; kinetic and thermodynamic approach. *Journal of Hazardous Materials*, 427, 127902. <https://doi.org/10.1016/j.jhazmat.2021.127902>
- Salim, N. A. A., Puteh, M. H., Khamidun, M. H., Fulazzaky, M. A., Abdullah, N. H., Yusoff, A. R. M., Zaini, M. A. A., Ahmad, N., Lazim, Z. M., Nuid, M. (2021). Interpretation of isotherm models for adsorption of ammonium onto granular activated carbon. *Biointerface Res. Appl. Chem*, 11, 9227-9241. <https://doi.org/10.33263/BRIAC112.92279241>
- Salimi, F., Tahmasobi, K., Karami, C., Jahangiri, A. (2017). Preparation of modified nano-SiO₂ by bismuth and iron as a novel remover of methylene blue from water solution. *Journal of the Mexican Chemical Society*, 61(3), 250-259. [chrome-extension://efaidnbmnnnibpcajpcglclefindmkaj/https://www.scielo.org.mx/pdf/jmcs/v61n3/1870-249X-jmcs-61-03-00250.pdf](https://www.scielo.org.mx/pdf/jmcs/v61n3/1870-249X-jmcs-61-03-00250.pdf)
- Tara, N., Sharma, A., Choudhry, A., Abdulla, N. K., Rathi, G., Khan, A. M., Chaudhry, S. A. (2021). Graphene, graphene oxide, and reduced graphene oxide-based materials: a comparative adsorption performance, in: Ahamad, A., Siddiqui, S.I. and Singh, P. (Eds.), *Contamination of Water*. Elsevier, Amsterdam, Netherlands, pp. 495-507. <https://doi.org/10.1016/B978-0-12-824058-8.00014-1>
- Verma, S., Dutta, R. K. (2020). Adsorptive Removal of Toxic Dyes Using Chitosan and Its Composites, in: Naushad, Mu., Lichtfouse, E. (Eds.), *Green Materials for Wastewater Treatment*. Springer, Berlin, Germany, pp. 223-255. DOI:10.1007/978-3-030-17724-9_10
- Wan, X., Rong, Z., Zhu, K., Wu, Y. (2022). Chitosan-based dual network composite hydrogel for efficient adsorption of methylene blue dye. *International Journal of Biological Macromolecules*, 222, 725-735. <https://doi.org/10.1016/j.ijbiomac.2022.09.213>
- Wang, H., Luo, W., Guo, R., Li, D., Xue B. (2022). Effective adsorption of Congo red dye by magnetic chitosan prepared by solvent-free ball milling. *Materials Chemistry and Physics*, 292, 126857. <https://doi.org/10.1016/j.matchemphys.2022.126857>
- Wong, S., Ghafar, N. A., Ngadi, N., Razmi, F. A., Inuwa, I. M., Mat, R., Amin, N. A. S. (2020). Effective removal of anionic textile dyes using adsorbent synthesized from coffee waste. *Scientific reports*, 10(1), 1-13. | <https://doi.org/10.1038/s41598-020-60021-6>
- Xu, K., Li, L., Huang, Z., Tian, Z., Li, H. (2022). Efficient adsorption of heavy metals from wastewater on nanocomposite beads prepared by chitosan and paper sludge. *Science of The Total Environment*, 846, 157399. <https://doi.org/10.1016/j.scitotenv.2022.157399>
- Yeo, J. Y. J., Khaerudini, D. S., Soetaredjo, F. E., Waworuntu, G. L., Ismadji, S., Putranto, A., Sunarso, J. (2023). Experimental and modelling study of adsorption isotherms of amoxicillin, ampicillin and doripenem on bentonite-chitosan composite. *South African Journal of Chemical Engineering*, 43, 38-45. <https://doi.org/10.1016/j.sajce.2022.09.013>
- Yun, J., Zhao, C., Li, X., Zhang, W., Liu, H., Liu, B. (2022). Rheological properties and early mechanical strength of oil-well cement modified by hybrid nano-silica and nano-hexagonal boron nitride. *Construction and Building Materials*, 356, 129291. <https://doi.org/10.1016/j.conbuildmat.2022.129291>
- Zaini, M. S. M., Arshad, M., Syed-Hassan, S. S. A. (2022). Adsorption Isotherm and Kinetic Study of Methane on Palm Kernel Shell-Derived Activated Carbon. *Journal of Bioresources and Bioproducts*, 8, 66-77. <https://doi.org/10.1016/j.jobab.2022.11.002>
- Zhao, S., Li, Y., Wang, M., Chen, B., Zhang, Y., Sun, Y., Chen, K., Du, Q., Wang, Y., Pi, X., Jing, Z., (2023). Efficient adsorption of Congo red by micro/nano MIL-88A (Fe, Al, Fe-Al)/chitosan composite sponge: Preparation, characterization, and adsorption mechanism. *International Journal of Biological Macromolecules*, 124157. <https://doi.org/10.1016/j.ijbiomac.2023.124157>
- Zhao, X., Wang, X., Lou, T. (2021). Preparation of fibrous chitosan/sodium alginate composite foams for the adsorption of cationic and anionic dyes. *Journal of Hazardous Materials*, 403, 124054. <https://doi.org/10.1016/j.jhazmat.2020.124054>